Chapter 5

Luminescence properties and energy transfer studies in thermally stable Bi_2O_3: Sm^{3+}, Eu^{3+} phosphor

The advent of innovative rare-earth based metal oxide phosphors has prompted increasing interest in the quest for highly efficient red emitting phosphors for various optoelectronic devices, lighting and display applications and motivated the research community to develop some promising, state-of-the-art, and potential red phosphors to meet the necessary requirements. In this chapter, a series of Sm^{3+} (1-7 mol %) doped, Sm^{3+} (5%) doped and Eu^{3+} (2-5 mol %) co-doped Bi_2O_3 red phosphors were synthesized by a facile urea assisted auto-combustion process. The X-ray diffraction (XRD) analysis of the phosphors ascertains the tetragonal crystal structure without any trace of impurity. The UV-Vis-NIR absorption study of the phosphors was carried out in 200-1000 nm range and the estimated optical band gap of the phosphors was lying in the range of 2.778 to 2.831 eV. The photoluminescence (PL) emission studies were performed at an excitation wavelength of 481 nm in the 550-720 nm range. The effective energy transfer mechanism from Sm^{3+} to Eu^{3+} in the Bi_2O_3 phosphor has been ascribed to the dipole-dipole (d-d) interaction. The energy transfer process was further validated by PL decay time measurements. The CIE color coordinates were obtained using PL emission data. The CIE chromaticity diagram ascertains that the emission color of Bi_2O_3: Sm^{3+} phosphors were tuned from reddish-orange to the red region by varying the concentration of Eu^{3+} ions. The temperature dependent PL study of the phosphors was taken out in the range of 293-453K and was found thermally stable at elevated temperatures.

5.1. Introduction

Over the past few decades, energy transfer studies in various rare-earth ion co-doped phosphors have been intensified for its use in color tunable light emission, white light emitting diodes, solar cells, and other lighting and display devices. For example, W. Sun *et al.* have studied the green to red color tunability via energy transfer from Tb^{3+} to Eu^{3+} in $Sr_8MgY(PO_4)_7$ phosphor [154]. Y. Wang *et al.* have discussed the energy transfer from Sm^{3+} to Eu^{3+} in $YAlO_3$ single crystal for enhancement in orange-red broadband [155]. P. Dixit *et al.* have synthesized Dy^{3+}, Sm^{3+} co-doped $CaMoO_4$ phosphors to realize neutral white light emission [156]. S. Gauhar *et al.* have prepared $Sr_6Ca_4(PO_4)_6F_2$ based red phosphors and discussed the energy transfer dynamics from Sm^{3+} to Eu^{3+} ions for white light emitting diodes and display devices [157]. The energy transfer studies from Pr^{3+} to Gd^{3+} in $Li(Lu,Gd)SiO_4:Pr^{3+},Sm^{3+}$ persistent phosphors have been carried out by S. Yan *et al.* for the application in optical tagging [158]. Moreover, the energy transfer from Cr^{3+} to Yb^{3+} in $K(Ga/Al)_{11}O_{17}$ phosphors was described by Z. Wang *et al.* for solar cell applications [159].

Rare-earth ions are used as activators and sensitizers in different host matrices and play a vital role in the emission enhancement and energy transfer processes. Generally, the rare earth ions exhibit three types of optical transitions namely intra-configurational 4f-4f transition, inter-configurational 4f-5d transition, and metal to ligand or ligand to metal charge transfer transition. Since, the 4f orbital electrons are screened by 5s and 5p orbitals, the 4f-4f transitions are less influenced by the crystal field environment of the host lattice and exhibit narrow emission lines. Moreover, the 5d orbital in 4f-5d transitions are strongly affected by the crystal field and exhibit broad emission bands [51]. Among various rare-earth ions, Sm^{3+} and Eu^{3+} are widely studied rare-earth ions owing to their prominent narrow emission bands in the reddish-orange part of the visible spectrum. There are several similarities between Sm^{3+} and Eu^{3+} ions such as the ionic radii of Sm^{3+}

and Eu^{3+} ions lie in proximity to each other. Also, the prominent emission band of both the phosphors lies in the red region of the visible spectrum. Moreover, the energy difference between $4_{G_{5/2}}$level of Sm^{3+} and 5_{D_0} level of Eu^{3+} is very small (~600 cm^{-1}). These properties make the above two rare earth ions as suitable dopants for effective energy transfer (from $4_{G_{5/2}} \rightarrow 5_{D_0}$) and improving the visible red emission in various host lattices.

A number of choices of host lattice are available for rare-earth based phosphors such as metal oxides, nitrides, molybdates, borates, phosphates, vanadates, sulphides, tungstates, silicates and so on [72,81,160–165]. Among them, metal oxides have shown potential to serve as suitable luminescence host owing to their excellent features and ease of synthesis. In recent years, bismuth oxide (Bi_2O_3) has dragged huge attention of the research community owing to its multifarious applications viz. photo catalysis, fuel cells, gas sensors, optoelectronics and optical coatings [109]. It is a wide band gap semiconductor and exhibit several remarkable features such as high oxygen-ion conductivity, high refractive index, dielectric permittivity, photo catalytic activity, chemical and thermal stability. Bi_2O_3 crystallizes in various polymorphic forms such as α (monoclinic), β (tetragonal), γ (BCC), δ (FCC), and ω (triclinic) etc. [166]. The properties of Bi_2O_3 phosphors are very unique such as it provides high quantum yield, and emits light across a broad range of wavelengths, from the visible to near-infrared region. Moreover, these phosphors are stable at high temperatures and considered to be relatively safe, non-toxic, and abundant material which is relatively inexpensive to synthesize. These properties make Bi_2O_3 phosphors a cost-effective choice where bright, long-lasting light is needed and also useful for a wide variety of applications including high temperature sensing, lighting, displays, and biomedical applications such as fluorescence imaging and diagnostics. Therefore, Bi_2O_3 phosphors offer many advantages that make them a

desirable choice for a variety of applications, particularly those that require high luminescence efficiency, broad emission spectra, thermal stability, non-toxicity, and low cost synthesis.

Much effort has been made for the synthesis of Bi_2O_3 based nanomaterials. W. Raza *et al.* have employed sol-gel method to synthesize La and Er doped Bi_2O_3 phosphors [109]. The co-precipitation synthesis Sm^{3+} doped Bi_2O_3 phosphors have been carried out by J. Divya *et al.*[54]. L. Fan *et al.* have prepared rare earth doped Bi_2O_3 phosphors via solid state method [53]. S. Ashwini *et al.* have used ultrasonication route for the synthesis of Li/Eu co-doped Bi_2O_3 phosphors [86]. The preparation of Bi_2O_3 was carried out via a citric method by L. Shan *et al.* [67]. We have preferred urea assisted auto combustion process as a prevalent method of phosphor synthesis over other conventional synthesis routes owing to its viable, lucrative, momentous, low-operating temperature, and environment-friendly nature [167].

In this chapter, the luminescence properties, decay mechanism and thermal stability of Sm^{3+} and Eu^{3+} co-doped Bi_2O_3 phosphors have been depicted for the first time. Moreover, a special attention has been devoted in the thorough investigation of energy transfer phenomenon from Sm^{3+} to Eu^{3+} ions.

5.2 Experimental methods

In this chapter, the urea assisted auto-combustion process has been utilized to prepare undoped, a series of Sm^{3+} (1-7 mol %) doped, and Sm^{3+} (5%) doped, Eu^{3+} (2-5 mol %) co-doped Bi_2O_3 phosphors and given the code names Sm0, Sm1, Sm3, Sm5, Sm7, SE2, SE3, SE4, and SE5, respectively. The starting materials employed in the synthesis were $Bi(NO_3)_3 \cdot 5H_2O$ (Sigma-Aldrich, 98%), $Sm(NO_3)_3 \cdot 6H_2O$ (Sigma-Aldrich, 99.9%), $Eu(NO_3)_3 \cdot 6H_2O$ (Thermo-Scientific 99.9%), and urea (Thermo-Scientific 99%) etc. The

stoichiometric proportion of rare-earth nitrates and bismuth nitrate pentahydrate were taken in a clean beaker and desired amount of HNO_3 was added in it. The solution was constantly stirred at 50 ^oC for 1 hour to get a homogeneous solution. Calculated amount of urea was added to this solution with constant stirring to ensure proper mixing. Now, the temperature was raised to 250 ^oC and the reaction mixture was left for 12 hours for combustion. The obtained material was grinded and powdered and then calcined at 600 ^oC for 4 hours in a furnace.

5.3 Characterizations

The XRD spectrum was recorded with the help of powder X-ray diffractometer (Rigaku miniflex-600 desktop), equipped with a Cu-K_α monochromatic source of radiation (λ=0.15406 nm) over the scan range of 2θ = 20-70^o, with operating current of 15 mA and voltage 30 kV. The X-ray photoelectron spectroscopic (XPS) analysis was accomplished using Thermo Fisher Scientific k-alpha X-ray photoelectron spectrometer. The vibrational modes and functional groups of the phosphors were probed using the JASCO FT/IR 4600 in the range 4000-400 cm^{-1}. The UV- Vis absorption spectroscopic measurements were taken out using JASCO V-770 spectrophotometer in the scan range 200-1000 nm. The PL measurements were performed with fluorescence spectrometer (Horiba scientific Fluorolog-3) attached with a 450 W xenon flash lamp and the FS5 spectrofluorometer (Edinburgh instruments) was employed to record the luminescence decay curves of the samples.

5.4 Results and discussion

5.4.1 Structural study

The X-ray diffraction (XRD) analysis was carried out to determine the crystal structure and authenticate the phase purity of the synthesized phosphors. Fig. 5.1 displays the stacked powder XRD patterns of undoped, Sm^{3+} (5%) doped, and Sm^{3+} (5%) doped, Eu^{3+}

(3%) co-doped Bi_2O_3 phosphors over the scan range of $20^o \leq 2\theta \leq 70^o$. The diffraction peaks were found consistent with the JCPDS card no. 78-1793, match well with the standard Bragg's position of tetragonal crystal structure of Bi_2O_3, and also no other impurity peaks were detected. The sharply defined peaks signify the high crystallinity of the samples and also suggest that the co-doping process does not lead to any modification in the crystal structure of the samples. The Scherrer's equation was employed to calculate the average crystallite size of the phosphors [103,144],

$$D = \frac{K\lambda}{\beta cos\theta} \tag{5.1}$$

Here, K is shape factor, λ is the wavelength of incident X-rays, β is the full width at half maxima (FWHM) in radian, and θ is the scattering angle. The estimated crystallite size values were lying in the range of 38-51 nm. The improvement in crystallinity of the phosphors upon incorporation of rare earth ions can be attributed to the following reasons: Sm^{3+} and Eu^{3+} ions are both trivalent rare earth ions, and their incorporation into the host crystal lattice can lead to structural stabilization. This can reduce lattice defects, increase crystallographic ordering, and improve the overall crystallinity of the material. Moreover, Both Sm^{3+} and Eu^{3+} ions are luminescent centres, meaning that they emit light when excited by a light source. This luminescence can induce crystallization in materials, as the emission of light can trigger the formation of ordered crystal structures.

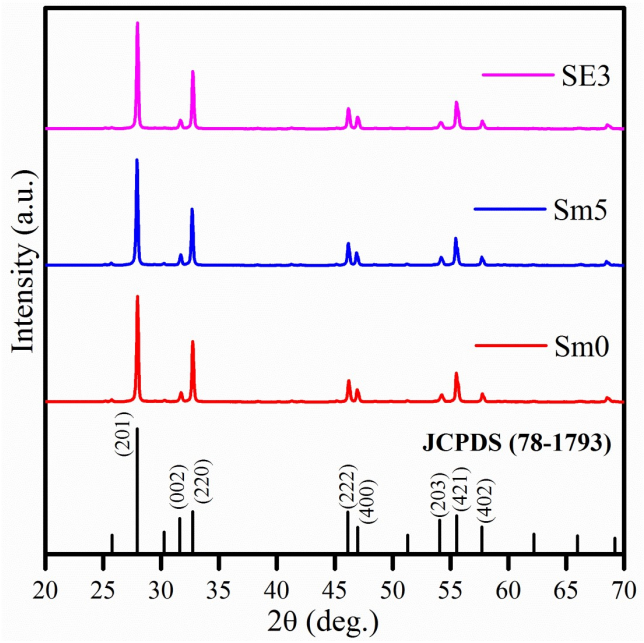

Fig. 5.1 Stacked XRD patterns of undoped, (5%) Sm^{3+} doped, (5%) Sm^{3+} and (3%) Eu^{3+} co-doped Bi_2O_3 phosphors.

5.4.2 XPS study

XPS is a surface sensitive tool probed for chemical analysis and elemental confirmation. It is also used to estimate the oxidation state of the chemical constituents present in the sample. Fig. 5.2 (a-e) displays the XPS spectra of SE3 phosphor. All the binding energy peaks were charge corrected using C 1s peak (B.E.= 284.7 eV) as the reference [67]. XPSPEAK41 software was implemented to fit the peaks and the peaks were fitted with Gaussian-Lorentzian fitting function along with Shirley-type background subtraction method. The prominent peaks corresponding to Bi, Sm, Eu and O in the XPS survey scan (depicted in Fig. 5.2 (a)) reveal the presence of all the elements in the samples. The peaks located at binding energies 158.4 and 163.7 eV were assigned to Bi $4f_{7/2}$ and Bi $4f_{5/2}$, respectively (Fig. 5.2 (b)), authenticating that Bi ions are present in +3 oxidation state in the sample [168]. Fig. 5.2 (c) exhibits the core level XPS spectrum of O 1s and resolved into two peaks centred at 528.9 and 530.7 eV corresponding to lattice oxygen (O_L) bonded to Bi-O unit and oxygen vacancies (O_V), respectively and manifest -2 oxidation state of

oxygen ions in the phosphors [69,128]. In Fig. 5.2 (d), the peaks appearing at 1109.7 and 1083.1 eV are attributed to Sm $3d_{3/2}$ and Sm $3d_{5/2}$, respectively and corroborate +3 oxidation state of Sm ions in the phosphors [54]. The high resolution XPS spectrum of Eu 3d is illustrated in Fig. 5.2 (e). The bands situated at 1163.9 and 1133.6 are assigned to Eu $3d_{3/2}$ and Eu$3d_{5/2}$ and consistent with +3 oxidation state of Eu ions [64].

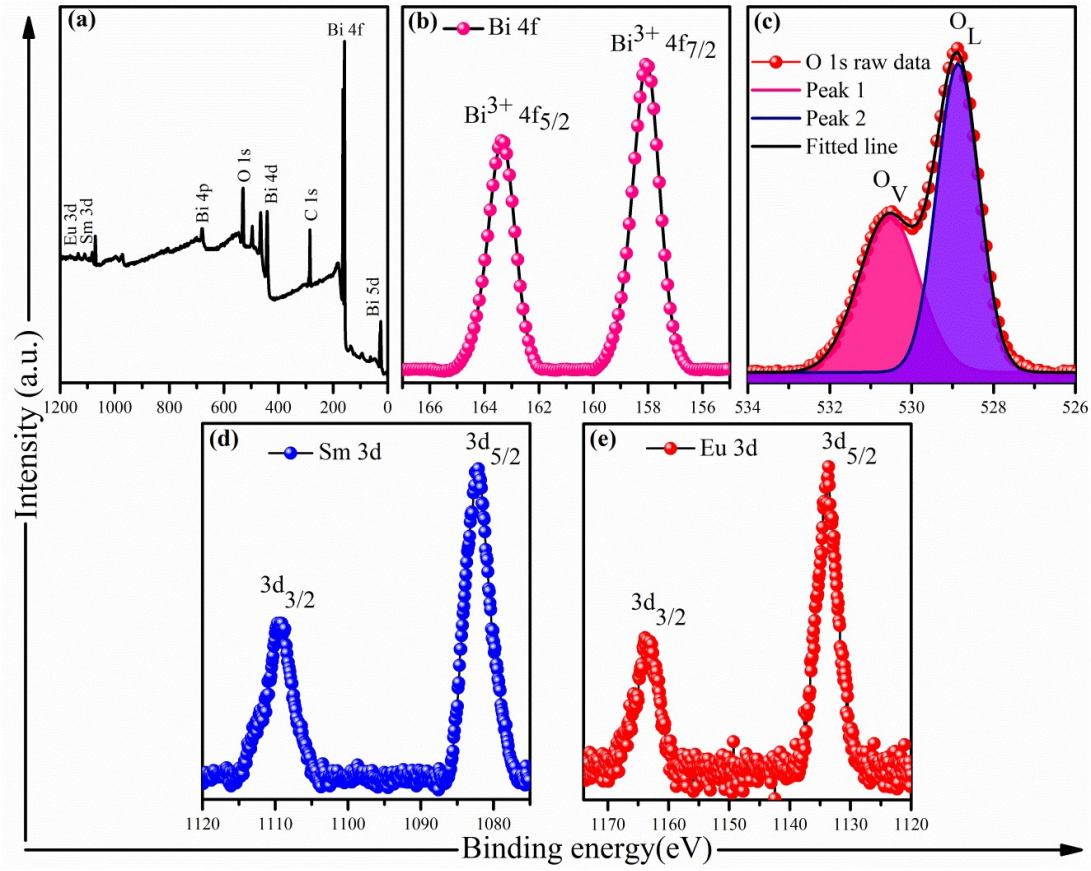

Fig. 5.2 (a) XPS survey scan, and high resolution XPS spectrum of **(b)** Bi 4f **(c)** O 1s **(d)** Sm 3d, and **(e)** Eu 3d in SE3 phosphor.

5.4.3 FTIR analysis

The Fourier transform infrared spectroscopy (FTIR) was probed to explore the vibrational modes and functional groups in the phosphors. Fig. 5.3 displays the FTIR spectra of Sm0, Sm5, and SE3 phosphors over the range of 400-4000 cm^{-1}. The IR bands located around 430, and 510 cm^{-1} are attributed to the characteristic Bi-O stretching vibration [134,169]. In

addition, the peak appearing at 550 cm^{-1} is ascribed to Bi-O-Bi vibration [137]. The small band situated near 1365 cm^{-1} represents the existence of nitrate functional groups, which may arise due to the presence of nitrate ions in the dopants and precursors [137,138]. Moreover, the existence of peaks around 1700 and 2360 cm^{-1} correspond to bending vibration of adsorbed water and atmospheric CO_2, respectively [138,140,170].

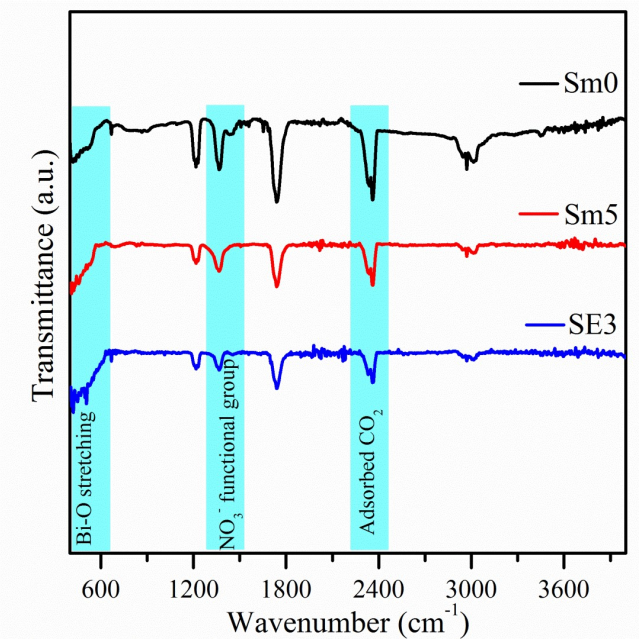

Fig. 5.3. FTIR spectra of Sm0, Sm5, and SE3 phosphors.

5.4.4 Absorption analysis

The UV-Vis-NIR absorption spectra of the synthesized doped and co-doped phosphors over the range of 200-1000 nm are presented in Fig. 5.4 (a, c). The direct allowed optical band gap values of the phosphors were determined using Wood and Tauc relation [171],

$$(\alpha h\nu)^2 = B(h\nu - E_g) \tag{5.2}$$

Where α, $h\nu$, and B are absorption coefficient, incident photon energy, and a constant, respectively. The corresponding Tauc plots are shown in Fig. 5.4 (b, d). The Tauc plots were fitted linearly and its intersection on the X-axis provides the required value of band

gap. The obtained band gap values are listed in Table 5.1. The values suggest that the incorporation of Sm^{3+} and Eu^{3+} ions in the host matrix leads to a reduction in the band gap. This may be due to the formation of additional trap levels corresponding to these ions between the conduction and valance band region. The Sm^{3+} and Eu^{3+} ions have different energy levels and electronic configurations than the host lattice ions, and when they are introduced into the phosphor material, they can create localized energy states within the band gap. These localized energy states can trap electrons, which can jump to higher energy states and emit light upon returning to their original energy level. This process results in the emission of visible light, which can be seen as a decrease in the band gap of the phosphor material.

Table 5.1. Variation of optical band gap with doping and co-doping concentration.

Sample code	**Optical band gap energy (E_g) (eV)**
Sm0	2.831
Sm1	2.803
Sm3	2.800
Sm5	2.799
Sm7	2.787
SE2	2.785
SE3	2.782
SE4	2.781
SE5	2.778

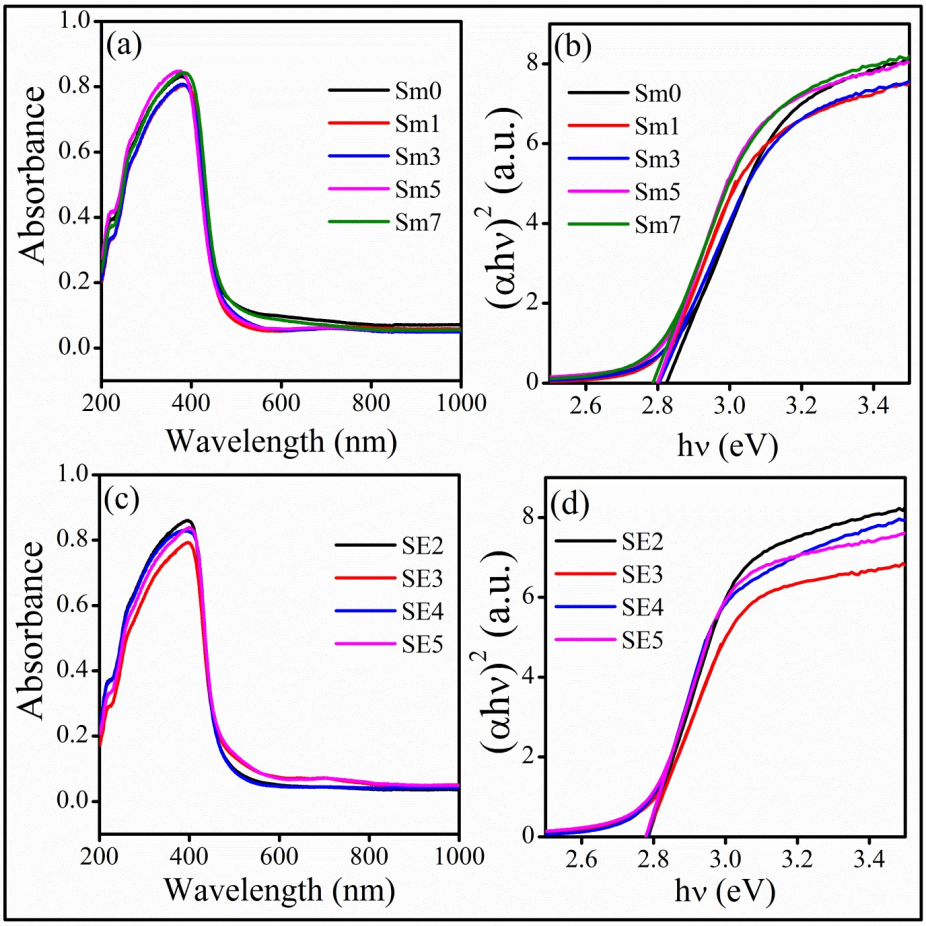

Fig. 5.4. (a, c) Absorption spectra, and **(b, d)** corresponding Tauc plots of synthesized phosphors.

5.5 PL study

Fig. 5.5 (a, b) depicts the room temperature PL excitation (PLE) spectra of Sm^{3+} (1-7%) doped Bi_2O_3, and Sm^{3+} (5%) doped, Eu^{3+} (2-5%) co-doped Bi_2O_3 phosphors at an emission wavelength of 598 nm, and Fig. 5.5 (c) shows the PLE spectra of the co-doped phosphors monitored at 612 nm emission wavelength and recorded over the range of 360-500 nm. The peaks in the spectra at 366, 406, 441, 468, 474, 481 nm wavelengths correspond to $(6_{H_{5/2}} \rightarrow 4_{D_{3/2,\ 5/2}})$, $(6_{H_{5/2}} \rightarrow 4_{F_{7/2}})$, $(6_{H_{5/2}} \rightarrow 4_{G_{9/2}})$, $(6_{H_{5/2}} \rightarrow 4_{I_{13/2}})$, $(6_{H_{5/2}} \rightarrow 4_{I_{11/2}})$, and $(6_{H_{5/2}} \rightarrow 4_{I_{9/2}})$ transitions of Sm^{3+} ion, respectively. Moreover, at 612 nm emission wavelength some excitation peaks at 450 $(7_{F_0} \rightarrow 5_{G_5})$, and 466 nm

($7_{F_0} \rightarrow 5_{D_2}$) corresponding to Eu^{3+} ion are also observed. Among them, the most prominent peak lies at 481 nm and was used to record the PL emission spectra of the phosphors. All the observed peaks in the spectra were found in agreement with the literature.

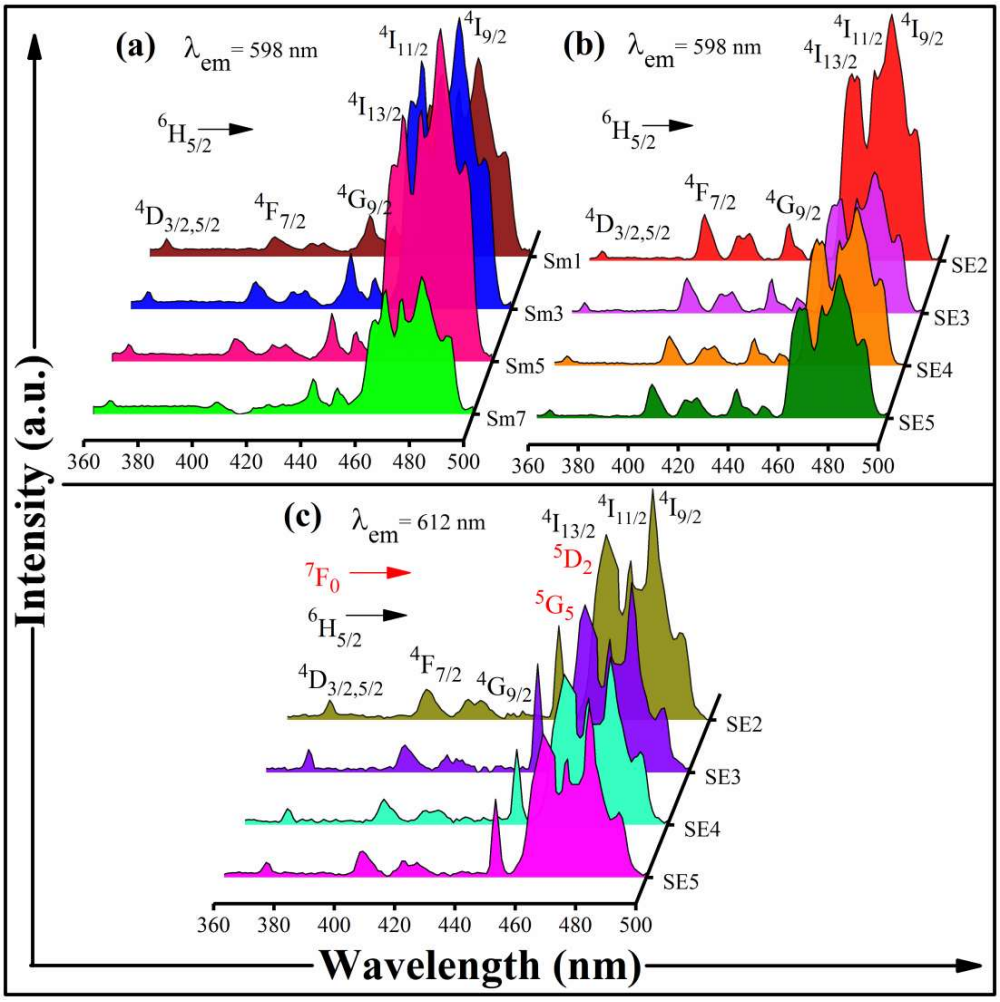

Fig. 5.5. PL excitation (PLE) spectra of **(a)** Sm^{3+} doped, **(b)** Sm^{3+}/Eu^{3+} co-doped Bi_2O_3 phosphors at 598 nm emission wavelength, and **(c)** Sm^{3+}/Eu^{3+} co-doped Bi_2O_3 phosphors at 612 nm emission wavelength.

Fig. 5.6 (a, b) shows the room temperature PL emission spectra of Sm^{3+} (1-7%) doped Bi_2O_3, and Sm^{3+} (5%) doped, Eu^{3+} (2-5%) co-doped Bi_2O_3 phosphors at an excitation wavelength of 481 nm in the range of 550-720 nm. The emission bands positioned at 562 ($4_{G_{5/2}} \rightarrow 6_{H_{5/2}}$), 598 ($4_{G_{5/2}} \rightarrow 6_{H_{7/2}}$), and 645 nm ($4_{G_{5/2}} \rightarrow 6_{H_{9/2}}$) are

assigned to characteristic 4f-4f emission bands of Sm^{3+} ion whereas the bands at 612 ($5_{D_0} \rightarrow 7_{F_2}$) and 698 nm ($5_{D_0} \rightarrow 7_{F_4}$) correspond to Eu^{3+} transition. The photoluminescence properties of Sm^{3+} and Eu^{3+} single doped Bi_2O_3 phosphors have been reported in detail in our earlier reports [103,170].

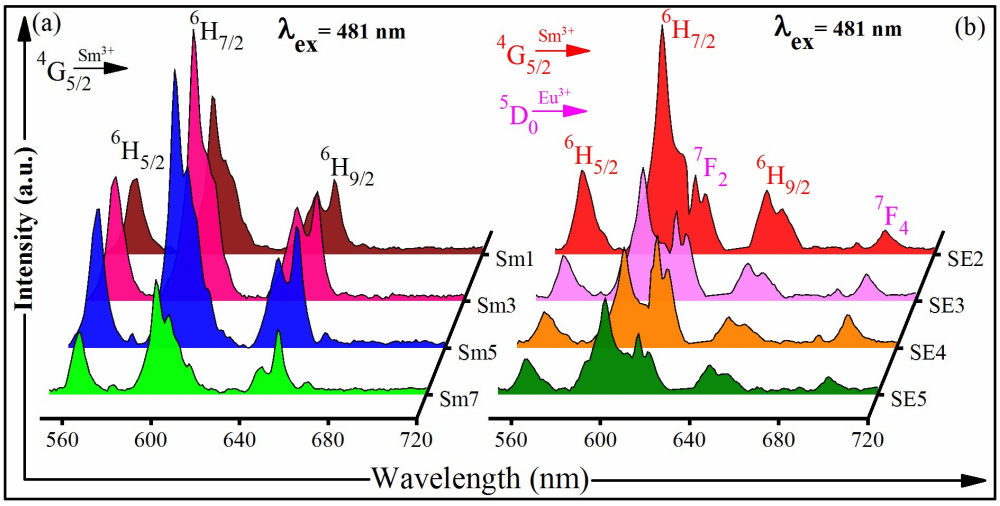

Fig. 5.6. PL emission spectra of **(a)** Sm^{3+} doped, and **(b)** Sm^{3+}/Eu^{3+} co-doped Bi_2O_3 phosphors at 481 nm excitation wavelength.

5.5.1 Energy Transfer Mechanism

To study the energy transfer mechanism between the rare earth ions, the Sm^{3+} concentration was fixed at an optimum concentration of 5 mol% and the Eu^{3+} content was varied between 2-5 mol%. It is observed that the intensity of emission peaks increases with increase in Sm^{3+} doping concentration in the host matrix, attains a maximum value for Sm5 sample and then decreases with further increase in Sm^{3+} concentration. The decrease in emission intensity is ascribed to the concentration quenching. Thus, it is concluded that the optimum Sm^{3+} doping concentration in the Bi_2O_3 host matrix is 5%. The non-radiative energy transfer among the neighbouring rare-earth ions may take place either via exchange interaction or multipolar interaction. The exchange interaction occurs

when the critical distance (R_c) between the dopant ions is shorter than 5Å. The critical distance can be calculated using the Blasse relation [103],

$$R_c = \left(\frac{6V}{\pi x_c N}\right)^{\frac{1}{3}} \tag{5.3}$$

Where, V (= 337.57) is unit cell volume, N (= 4) is the number of available cation sites, and x_c (= 0.09) is the total critical concentration of Sm^{3+} and Eu^{3+} ions. The calculated value of R_c for SE3 phosphor comes out to be 9.11Å. This suggests that the exchange interaction is ineffective for non radiative energy transfer and it is governed by multipolar interaction. Electric multipolar interactions are classified into three types: dipole-dipole, dipole-quadrupole, and quadrupole-quadrupole [172]. The type of multipolar interaction involved in the energy transfer process can be estimated with the help of Dexter's formula and Reisfeld's approximation given as [173,174],

$$\frac{I_0}{I} \propto C^{n/3} \tag{5.4}$$

Where, I_0 and I are the emission intensities of Sm^{3+} with and without Eu^{3+} ions and C is the sum of doping concentrations of Sm^{3+} and Eu^{3+}. The plots of (I_0/I) vs. $C^{n/3}$ (Fig. 5.7 (a)) with n = 6, 8, and 10 correspond to dipole- dipole, dipole-quadrupole, and quadrupole- quadrupole interactions, respectively. The Fig. shows a linear behaviour and the best fitting was observed for n = 6. This confirms that the energy transfer mechanism from Sm^{3+} to Eu^{3+} is mainly due to the non-radiative dipole-dipole interaction.

From Fig. 5.6 (b), it can be observed that, as the doping concentration of Eu^{3+} ions increases, the intensity of emission peaks corresponding to Sm^{3+} decreases while the intensity of peaks corresponding to that of Eu^{3+} increases gradually. This suggests an effective energy transfer from Sm^{3+} to Eu^{3+} in Bi_2O_3 host [43].

The schematic energy level diagram depicting the probable energy levels and transitions involved in the luminescence phenomena and the energy transfer process from Sm^{3+} to Eu^{3+} in the Bi_2O_3 host matrix is illustrated in Fig. 5.7 (b).

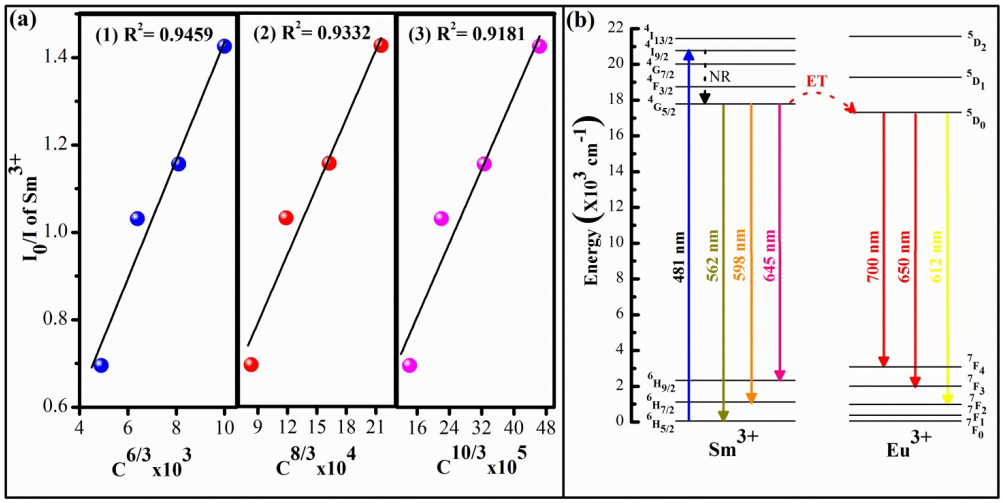

Fig. 5.7. (a) Dependence of I_0/I of Sm^{3+} ions on (1) $C^{6/3}$ (2) $C^{8/3}$, and (3) $C^{10/3}$ in Bi_2O_3:Sm^{3+}, Eu^{3+} phosphors, and **(b)** Schematic energy level diagram of Sm^{3+} and Eu^{3+} ions depicting the energy transfer process.

5.6 PL decay analysis

The normalized PL decay curves of $4_{G_{5/2}} \rightarrow 6_{H_{7/2}}$ energy level (598 nm emission) of Sm^{3+} ion at 481 nm excitation wavelength for Sm5 and SE3 phosphors are displayed in Figs. 5.8(a and b), respectively. The decay curves were fitted with a double-exponential function given as [150],

$$I(t) = I_0 + B_1 exp(-\ t/\tau_1\ ) + B_2 exp(-t/\tau_2) \qquad (5.5)$$

Where the intensities at time 0 and after t seconds are denoted by I_o and I; B_1 and B_2 symbolize the fitting constants; τ_1 denotes the fast and τ_2 denotes the slow decay time components, respectively. The following relation is used to evaluate the average lifetime of the phosphors [150],

$$\tau_{avg} = (B_1\tau_1^2 + B_2\tau_2^2)/(B_1\tau_1 + B_2\tau_2) \quad (5.6)$$

The calculated average lifetime of $4_{G_{5/2}}$ level of Sm^{3+} ion for Sm5 and SE3 phosphors were found to be 504 and 444 µs, respectively. The reduced value of lifetime in Eu^{3+} co-doped phosphors suggests an effective energy transfer from Sm^{3+} to Eu^{3+} ions.

The following equation can be used to calculate energy transfer efficiency [154,175],

$$\eta_{ET} = 1 - \frac{\tau_x}{\tau_o} \quad (5.7)$$

Where τ_x and τ_o are the average lifetime of $4_{G_{5/2}}$ level of the Sm^{3+} ion in SE3 and Sm5 phosphors, respectively. Consequently, the calculated η_{ET} value is 11.91%.

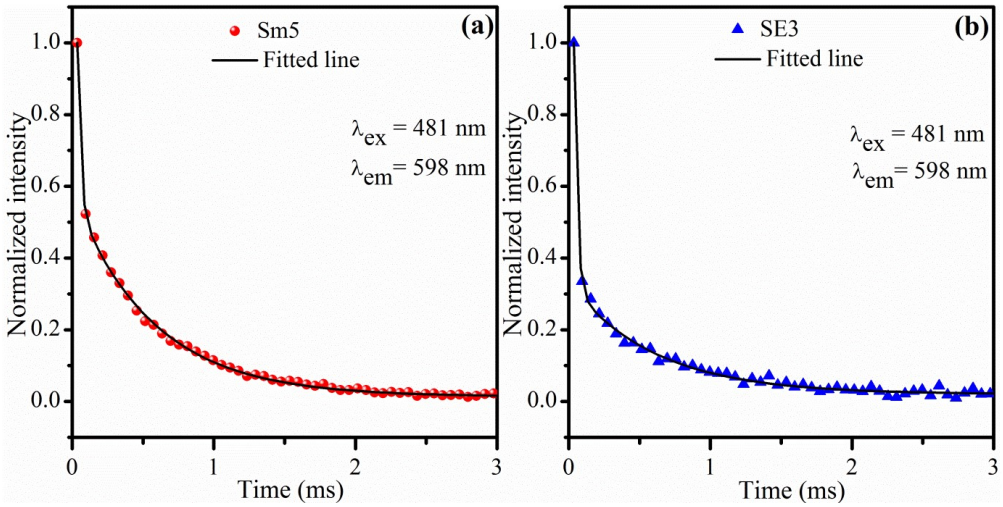

Fig. 5.8. Normalized lifetime decay curves of **(a)** Sm5, and **(b)** SE3 phosphors excited at 481 nm and monitored at 598 nm.

5.7 Thermal Stability

The temperature dependent PL is an essential study of the phosphors to investigate their thermal stability and temperature dependent emission properties for application in lighting devices. Herein, the temperature dependent emission spectra (Fig. 5.9 (a)) of

Sm^{3+} (5%) doped and Eu^{3+} (3%) co-doped Bi_2O_3 phosphor has been investigated at 481 nm excitation wavelength over the temperature range of 303-543 K at the intervals of 30 K. It can be seen from the spectra that with the increase in temperature the emission intensity declines gradually owing to the thermal quenching effect. At 423 K, the intensity reduced by 56.22% and becomes 43.78% of the initial emission intensity measured at 303 K (shown in Fig. 5.9 (b)), indicating that the synthesized Eu^{3+} co-doped phosphors have good thermal stability and they are potential candidates to realize efficient lighting and display devices. Moreover, the activation energy (E_a) is an important parameter to determine the thermal stability of the phosphors and can be calculated using the Arrhenius relation [175],

$$I_T = \frac{I_0}{1+Cexp(-E_a/KT)} \tag{5.8}$$

Where I_0 is the PL intensity at 303 K and I_T is the intensity at different testing temperatures; C is a constant and K is the Boltzmann's constant. Fig. 5.9 (c) depicts the linear fitting of $ln\left(\frac{I_0}{I_T}-1\right)$ vs. $1/KT$ plot and its slope provides the value of E_a. Consequently, the estimated value of E_a is 0.44 eV.

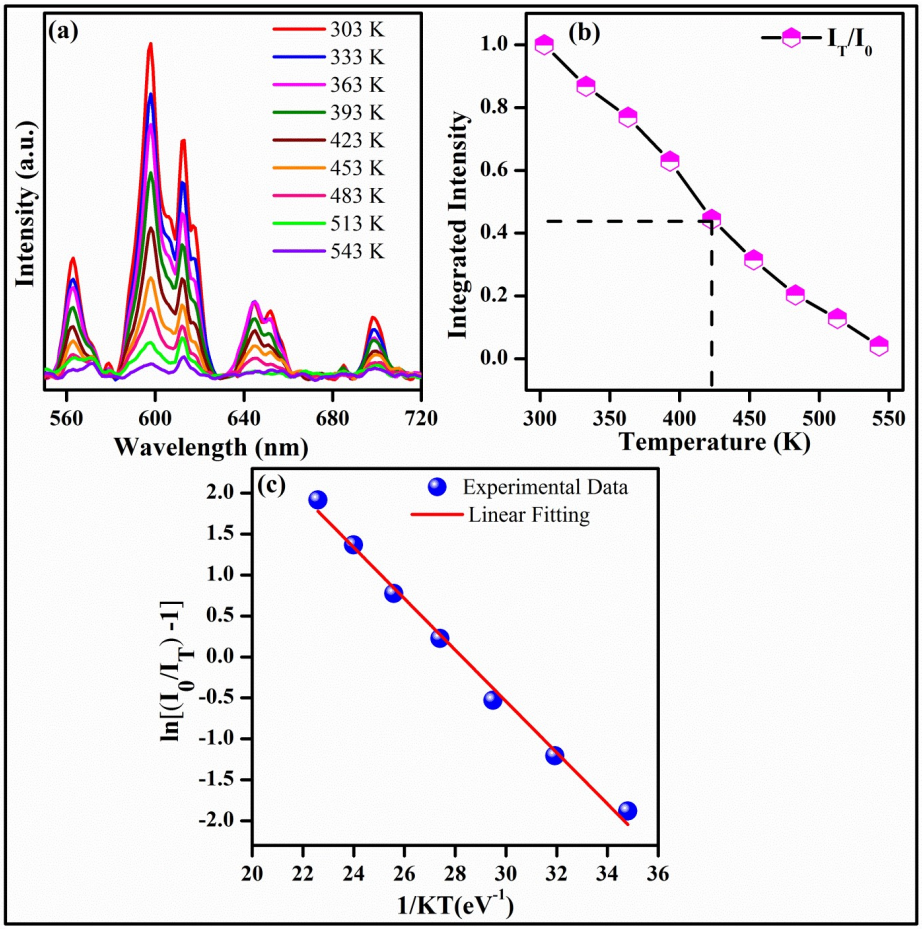

Fig. 5.9. (a) Temperature dependent emission spectra, **(b)** variation of normalized integrated intensity with temperature, and **(c)** $\boldsymbol{ln}\ [(\boldsymbol{I_0/I_T}) - \mathbf{1}]$ versus 1/KT plots for SE3 phosphor.

5.8 CIE and CCT analysis

The Commission internationale de I'Eclairage (CIE) chromaticity diagram of Sm5, SE2 and SE4 phosphors are depicted in Fig. 5.10. The correlated colour temperature (CCT) was calculated using the empirical McCamy equation [153],

$$\text{CCT} = 5520.33 - 6823n + 3525n^2 - 449n^3 \qquad (5.9)$$

Where (x, y) is the CIE coordinate, (x_e, y_e) is the chromaticity epicentre having coordinates (0.338, 0.186), and $n = \left(\frac{x-x_e}{y-y_e}\right)$ is the inverse slope line. The estimated CCT

values for Sm5, SE2 and SE4 were found to be 2260, 2088, and 1890 K, respectively, depicting an explicit red-shift with increase in co-doping concentration.

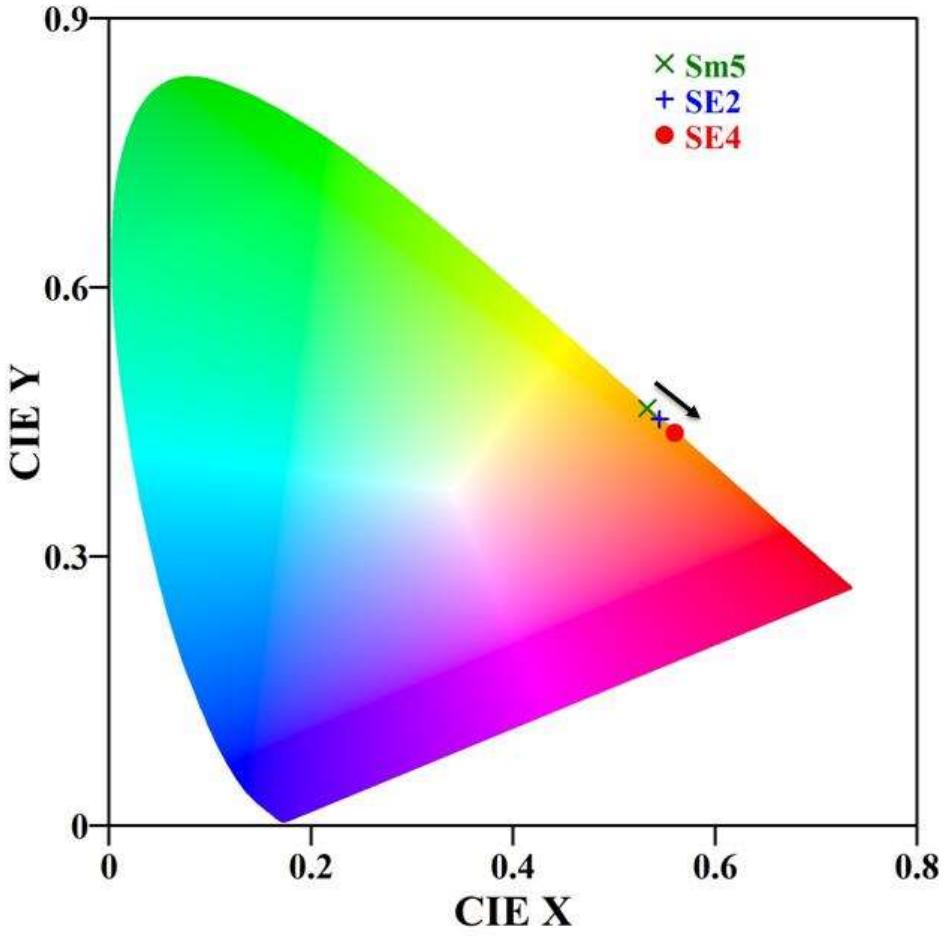

Fig. 5. 10 CIE chromaticity diagram showing the variation in CIE coordinates in the doped and co-doped phosphors for Sm5, SE2 and SE4 phosphors.

5.9 Conclusions

In summary, the present chapter provides study of a series of Sm^{3+}, Eu^{3+} co-doped Bi_2O_3 phosphors synthesized by a facile auto-combustion route. The study of structural, optical, and thermal stability of the phosphors have been carried out in detail. The XRD analysis corroborates that all the prepared phosphors have tetragonal crystal structure. An augmentation in the crystallinity of the phosphors has been observed with increase in

doping concentration. The XPS study reveals that all the elements are present in the samples in their respective oxidation states. The information regarding vibrational states and functional groups in the samples was provided by FTIR analysis. The UV-Vis-NIR absorption study suggests that the band gap of the phosphors decreases after doping and co-doping, which may arise due to the formation of additional trap states within the conduction and valance band region. The PL excitation and emission studies were carried out at 481 ($6_{H_{5/2}} \rightarrow 4_{I_{9/2}}$) nm excitation wavelength and 598 nm ($4_{G_{5/2}} \rightarrow 6_{H_{7/2}}$) emission wavelengths, respectively. The phenomena of energy transfer from Sm^{3+} to Eu^{3+} ions have been discussed thoroughly. The thermal stability of the phosphors was examined using temperature dependent PL analysis over the range of 303- 543 K. A significant shift in the CIE coordinates from orange to reddish-orange region was observed after Eu^{3+} co-doping in Sm^{3+} doped phosphors. Thus our study corroborates that, Sm^{3+} and Eu^{3+} co-doped Bi_2O_3 phosphors in proper composition can prompt effective energy transfer phenomena and are potential candidates to realize efficient and thermally stable lighting and display devices.